

This work was written as part of one of the author's official duties as an Employee of the United States Government and is therefore a work of the United States Government. In accordance with 17 U.S.C. 105, no copyright protection is available for such works under U.S. Law.

Public Domain Mark 1.0

<https://creativecommons.org/publicdomain/mark/1.0/>

Access to this work was provided by the University of Maryland, Baltimore County (UMBC) ScholarWorks@UMBC digital repository on the Maryland Shared Open Access (MD-SOAR) platform.

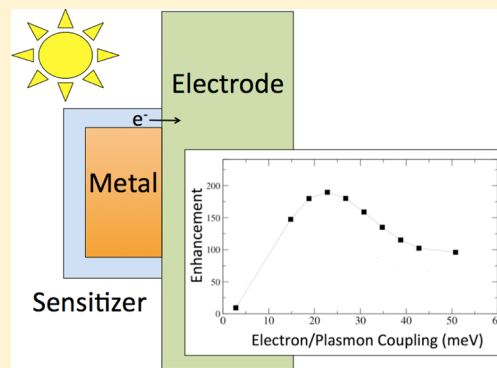
Please provide feedback

Please support the ScholarWorks@UMBC repository by emailing scholarworks-group@umbc.edu and telling us what having access to this work means to you and why it's important to you. Thank you.

Plasmon-Enhanced Electron Injection in Dye-Sensitized Solar Cells

S. Ramakrishna,[†] Matthew Pelton,[‡] Stephen K. Gray,[¶] and Tamar Seideman^{*,†}[†]Department of Chemistry, Northwestern University, 2145 Sheridan Road, Evanston, Illinois 60208-3113, United States[‡]Department of Physics, University of Maryland, Baltimore County, 1000 Hilltop Circle, Baltimore, Maryland 21250, United States[¶]Center for Nanoscale Materials, Argonne National Laboratory, 9700 South Cass Avenue, Argonne, Illinois 60439, United States

ABSTRACT: Recent experiments have shown that the efficiency of photoinduced electron transfer from sensitizers (molecules or quantum dots) to semiconductors can be enhanced by coupling the sensitizers to plasmon resonances in metal nanoparticles. Here, we use a model-Hamiltonian approach to show theoretically that there is an optimal coupling between the sensitizer and plasmons that maximizes the electron-transfer efficiency. This optimum results from the competition between electron transfer, plasmon relaxation, and plasmon decoherence. For coupling values that exceed the optimal value, the dynamics of electron transfer from the sensitizer to the semiconductor can be significantly modified due to the sensitizer–plasmon coupling.



■ INTRODUCTION

Plasmonic metal nanoparticles (MNPs) have been investigated as a means of enhancing the efficiency of solar cells by increasing the absorption of sunlight by the active material in the solar cell.¹ This has the potential to be particularly useful in solar cells where efficiency is limited by carrier transport and one would like to make the active layer as thin as possible, such as organic photovoltaics² and dye-sensitized solar cells (DSSCs).^{3,4} Although many of the reported enhancements in efficiency are simply caused by increases in optical path length due to scattering by the MNPs, experiments have indicated that the enhancement in certain DSSCs arises from near-field plasmonic effects,^{4–7} as have been identified to be important in enhancing many molecular optical processes.⁸ The importance of plasmonic effects has been verified theoretically for a specific multicomponent system by computations that employed both quantum mechanics and classical electrodynamics.⁹ Theoretical work has also been performed using a fully quantum-mechanical approach based on a model-Hamiltonian approach and employing a density-matrix formalism.^{10,11} This work investigated the efficiency of photoinduced electron transfer between the molecular chromophore (i.e., the photosensitizer) and the semiconductor, the primary charge-transfer step in DSSCs.^{12–14} The electron-transfer efficiency was seen to increase as the distance between the photosensitizer and the MNP was decreased.¹⁰ Using more than one MNP led to enhancement peaks as a function of excitation wavelength that varied for different geometries, indicating the possibility of designing optimum configurations.¹¹

These studies indicate that the enhancement of electron transfer is more complex than a simple, linear enhancement of optical absorption by the sensitizer due to the near field of the MNP and involves interaction among all the components of the

system. In this paper, we use a quantum Liouville equation approach to investigate how these interactions affect the dynamics of electron injection from the photosensitizer to the semiconductor. The approach also includes environmental dephasing and dissipation. We vary the magnitude of the dipole–dipole coupling between the plasmon resonance in the MNP and the electronic transition in the photosensitizer and find that the dynamics are indeed sensitive to this coupling strength. An optimum value of this coupling strength emerges, for which the electron population injected into the semiconductor electrode is maximized.

■ THEORETICAL METHODS

Figure 1a is a schematic image of the system under consideration, which involves molecular or quantum dot sensitizers in close proximity to a plasmonic system (e.g., one or more metal nanoparticles) and a semiconductor electrode. We employ a model-Hamiltonian approach, in which the electronic and plasmonic subsystems are both treated quantum mechanically, and their dynamics are described by a density-matrix formalism. The Hamiltonian of the electron–plasmon system interacting with a field is an extension of previous work¹⁵ to include electrode states, and can be expressed as

$$H = H_{\text{elec}} + H_{\text{plas-elec}} + H_{\text{field}} \quad (1)$$

where the electronic part (H_{elec}) consists of a two-level system representing the ground (m_g) and excited (m_e) states of a molecule or a quantum dot, a quasicontinuum of electronic levels (k) representing the conduction band levels of a semiconductor electrode, and coupling terms that allow for

Received: August 7, 2015

Published: September 4, 2015

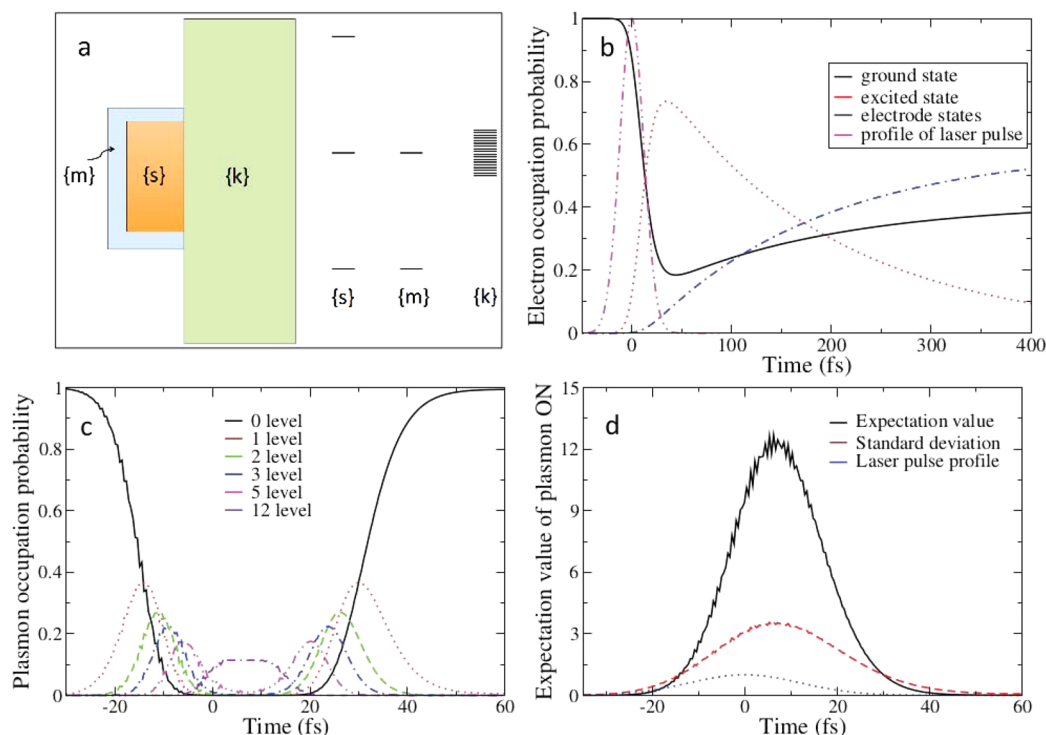


Figure 1. Laser-induced electron and plasmon population dynamics in a coupled photosensitizer–metal nanoparticle (MNP)–semiconductor system. (a) Schematic diagram of a sensitizer layer that may contain active dye molecules or quantum dots (blue), a plasmonic structure (orange), and semiconductor electrode (pale green). On the right-hand side are energy level ladders indicating the first few plasmonic (s) levels and the molecular (m) and semiconductor (k) levels. Results in panels b–d are shown for electron-transfer time $\tau_{el} = 261$ fs, electronic–plasmon coupling strength $\hbar g = 6.8$ meV, and plasmon relaxation $\hbar\gamma_s = 0.15$ eV. (b) Electronic populations of ground molecular (solid black), excited molecular (dotted red), and electrode (dot–dashed blue) states. The 20 fs laser pulse envelope, centered on $t = 0$, is also indicated (dot–dashed red curve). (c) Plasmon populations of the MNP: ground (solid black), first excited (dotted red), second excited (dashed green), third excited (dot–dashed blue), fifth excited (dot–dot–dashed magenta), and twelfth excited state (dot–dash–dashed violet). (d) Expectation value of the plasmon occupation number (ON) (black), along with its standard deviation (dashed red). The laser pulse envelope is again indicated (dotted blue curve).

electron transfer between the excited state of the two-level system and the semiconductor electrode (V_{km_e}). Explicitly

$$H_{elec} = \sum_k \epsilon_k |k\rangle \langle k| + \sum_{i=e,g} \epsilon_{m_i} |m_i\rangle \langle m_i| + \sum_k (V_{m_e k} |m_e\rangle \langle k| + V_{km_e} |k\rangle \langle m_e|) \quad (2)$$

where ϵ_j represent the electronic energies and $|j\rangle$ the state vectors of the two-level system ($j = m_g, m_e$) and of the electrode ($j = k$). The Hamiltonian of the plasmon and the plasmon–electronic coupling in a fully quantum description can be derived using a cavity quantum electrodynamics approach:¹⁶

$$H_{plas-elec} = \sum_s (s\hbar\omega_s |s\rangle \langle s| - \hbar g \sqrt{s+1} |m_g\rangle |s+1\rangle \langle s| \langle m_e| - \hbar g \sqrt{s} |m_e\rangle |s-1\rangle \langle s| \langle m_g|) \quad (3)$$

In the above, s is the plasmon quantum number, $\hbar\omega_s$ its energy, and $\hbar g$ is the coupling between the electronic and plasmon levels. The plasmons of the MNP are modeled as harmonic-oscillator (bosonic) states, analogous to photon states in an optical cavity. The coupling exists between electronic excitations and plasmon de-excitations and vice versa, rather than between simultaneous excitations and de-excitations, because the latter are nonresonant.¹⁵ Finally, the interaction of the incident electric field of the laser, $E(t)$, with both the

plasmons of the MNP and the electronic two-level system is described by a semiclassical Hamiltonian:

$$H_{field} = -E(t)\mu_m(|m_e\rangle \langle m_g| + |m_g\rangle \langle m_e|) - E(t) \sum_s \mu_s (\sqrt{s+1} |s+1\rangle \langle s| + \sqrt{s} |s\rangle \langle s+1|) \quad (4)$$

where μ_m and μ_s are the dipole transition moments associated with the two-level system and the plasmon, respectively.

The dynamics of the coupled system are governed by the quantum Liouville equation:

$$\frac{d\hat{\rho}}{dt} = -\frac{i}{\hbar} [H, \hat{\rho}] + L(\hat{\rho}) \quad (5)$$

where the density operator $\hat{\rho}$ describes a composite electron–plasmon state:

$$\hat{\rho} = \sum_{l,s,l',s'} \rho_{sl's',ll} |l\rangle \langle s'| \langle l'| \quad (6)$$

where $l = \{k, m_e, m_g\}$ and the dissipative part $L(\hat{\rho})$ is a Lindblad superoperator similar to the one in ref 15. Accordingly, the electronic two-level system has a pure electronic dephasing rate (γ_e^{pd}) and its excited state has a finite lifetime (γ_e)^{−1}, whereas the plasmon system undergoes energy relaxation and decoherence at a rate γ_s . Calculations are performed using the following parameters: $\epsilon_{m_e} - \epsilon_{m_g} = \hbar\omega_s = 2.042$ eV, $\mu_m = 13.9$ D, $\mu_s = 2990$ D, $\hbar\gamma_e = 268$ neV, and $\hbar\gamma_e^{pd} = 1.27$ meV.

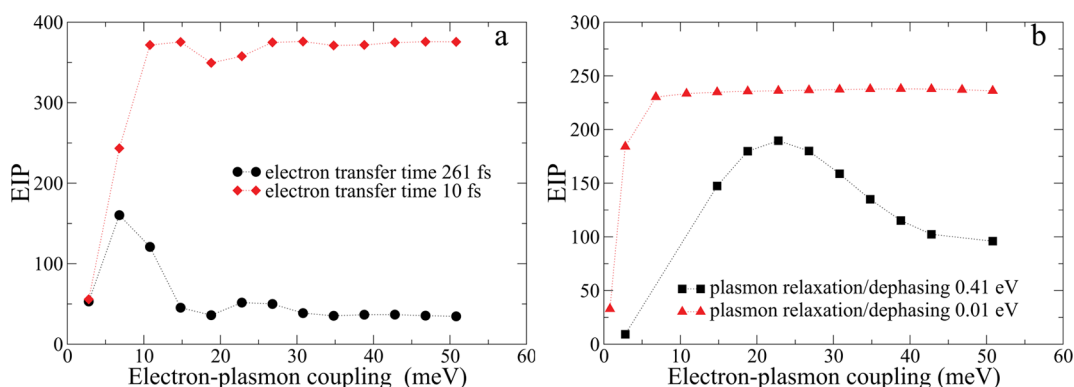


Figure 2. Enhancement of the injection probability (EIP) from the photosensitizer to the semiconductor as a function of the electron–plasmon coupling strength ($\hbar g$). (a) Plasmon relaxation, $\hbar\gamma_s = 0.15$ eV; black circles correspond to electron-transfer rate $\tau_{el} = 261$ fs, and red diamonds correspond to $\tau_{el} = 10$ fs. (b) $\tau_{el} = 50$ fs; black squares correspond to $\hbar\gamma_s = 0.41$ eV, and red triangles correspond to $\hbar\gamma_s = 0.01$ eV.

These values have been obtained using electrodynamics simulations for a quantum dot sandwiched between two gold MNPs, in the absence of an electrode.¹⁵ Similar values have been used in a model for a molecule attached to the surface of a TiO_2 layer with a spherical MNP close by.¹⁰ The values $\hbar g = 10.8$ meV and $\hbar\gamma_s = 150$ meV were obtained via a fitting procedure outlined in ref 15. As one focus of this work is on understanding how the electron injection yield and its dynamics depend parametrically on g and γ_s , these parameters will be varied over a wide range with a view to establishing limiting trends. The coupling strength, $\hbar g$, is related to the local-field intensity at the location of the sensitizer due to plasmons in the MNP and can thus be varied by changing the location of the sensitizer relative to the MNP. The variation of γ_s that is explored here, by contrast, may not be physically realizable but serves to illustrate the physical processes involved in modifying charge transfer in this coupled system.

Eighty substrate levels with a spacing of $\Delta = 10$ meV are chosen for the semiconductor electrode, amounting to a total conduction-bandwidth of 0.8 eV. ϵ_{m_e} is situated at the center of the band so as to exclude band-edge effects from the electron-injection process. The electronic coupling between the excited state and substrate levels ($V_{m,k}$) is assumed to be independent of energy. The electron population in the excited state decays in a monoexponential fashion to the substrate levels in the dark, long before it decays to the ground state. Its lifetime in the dark, τ_{el} ,¹⁷ given as

$$\tau_{el} = \frac{\hbar\Delta}{2\pi|V_{m,k}|^2} \quad (7)$$

will be varied in the calculations by varying $V_{m,k}$. The range of τ_{el} values explored here, $10 \leq \tau_{el} \leq 270$ fs, is typical of dye-sensitized solar cells.

RESULTS AND DISCUSSION

In order to investigate the injection dynamics, we excite the system with a short laser pulse, as would be done, for example, in a pump–probe optical measurement. A Gaussian laser pulse of 20 fs FWHM with a central energy of 2.042 eV and a maximum electric field of 10^7 V/m is used to excite the electronic–plasmonic system, which corresponds to a fluence of about 500 nJ/cm². The resulting dynamics are shown in Figure 1b–d. Figure 1b displays the molecular ground (black) and excited (dotted red) state populations as well as the total

population in the electrode levels (dot–dashed blue). We see electronic population transfer from the molecular ground state to the excited state, and from there to the electrode levels. The envelope of the laser pulse, centered at $t = 0$, is also shown for reference. The sensitizer–electrode coupling strength used in this calculation corresponds to $\tau_{el} = 261$ fs. The electrode-state population, or injection probability $IP = \sum_k \text{Tr}\{\hat{\rho}|k\rangle\langle k|\}$, fits to a monoexponential rise with a time constant of 261 fs rather accurately, except for the very initial period when the laser pulse is on. The slow rise in the ground electronic state long after the 20 fs fwhm laser pulse is gone is due to transfer from the electronic excited state that is facilitated by energy transfer between the plasmon and electronic subsystems.

Figure 1c shows the excitations of the different plasmon levels. To begin, as in the electronic subsystem, all plasmonic population is in the ground state. The laser pulse leads to excitations and, as the selection rules permit only nearest-neighbor transitions, the plasmon population gets transferred to higher and higher states in a successive fashion until it peaks around the 12th level in this case. (Many plasmon levels $s > 12$ are also populated, although to a somewhat smaller extent.) As the laser pulse dies down, de-excitation occurs, once again in a successive manner, as the final population returns to the ground state due to plasmon relaxation and dephasing. The relaxation is fast enough to suppress any oscillations in population between levels. Figure 1d depicts the corresponding expectation value of the plasmon occupation number operator along with its standard deviation, which is also consistent with significant plasmon occupancy during and slightly after the pulse.

To understand how the injection probability depends on the system parameters, we define the enhancement of injected probability (EIP) as the ratio $EIP(g, t_s) = IP(g, t_s) / IP(g = 0, t_s)$, where $IP(g, t_s)$ is the electrode population at a specific time t_s and $IP(g = 0, t_s)$ is the electrode population at the same time when the electronic–plasmonic coupling is absent.¹⁰ We set $t_s = 400$ fs because by this time the transfer is usually complete or nearly complete. In Figure 2a, we show two sets of data which differ from one another in the choice of the injection time, τ_{el} (eq 7), but share the same value for the plasmon relaxation/dephasing rate, γ_s . For the longer injection time ($\tau_{el} = 261$ fs), the injection efficiency initially rises with increasing electronic–plasmon coupling, $\hbar g$, reaching a maximum of about 160 for $\hbar g \approx 5$ meV. With further increases in $\hbar g$, the injection efficiency decreases, reaching a plateau at a value around 50 that persists

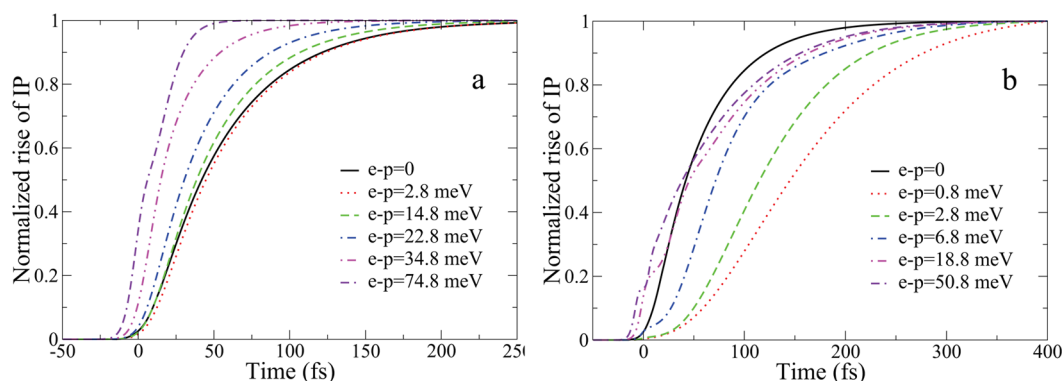


Figure 3. Dynamics of electron transfer to electrode or normalized injection probability (IP) for $\tau_{\text{el}} = 50$ fs. (a) $\hbar\gamma_s = 0.41$ eV: $g = 0$ (solid black), $\hbar g = 2.8$ meV (dotted red), $\hbar g = 14.8$ meV (dashed green), $\hbar g = 22.8$ meV (dot-dashed blue), $\hbar g = 34.8$ meV (dot-dot-dashed magenta), $\hbar g = 74.8$ meV (dot-dash-dashed violet). (b) $\hbar\gamma_s = 0.01$ meV: $g = 0$ (solid black), $\hbar g = 0.8$ meV (dotted red), $\hbar g = 2.8$ meV (dashed green), $\hbar g = 6.8$ meV (dot-dashed blue), $\hbar g = 18.8$ meV (dot-dot-dashed magenta), $\hbar g = 50.8$ meV (dot-dash-dashed violet).

up to large values of $\hbar g$. On the other hand, for a short electron-transfer time ($\tau_{\text{el}} = 10$ fs), the enhancement factor climbs sharply to higher values and plateaus around 375, without an apparent maximum.

In Figure 2b, we show results for two different plasmon lifetimes. When the plasmon relaxation/dephasing is very rapid, one finds an unambiguous optimum value of $\hbar g \approx 22.8$ meV, whereas when the plasmon relaxation/dephasing is much slower, the EIP values rise sharply with $\hbar g$ and, after a threshold value of $\hbar g = 6.8$ meV, saturates around 230. Overall, for a given electron transfer and plasmon lifetime, there is either an optimum value of $\hbar g$ for which one obtains maximum injection efficiency or a threshold $\hbar g$ value above which the EIP reaches a plateau.

The efficiency of population injection into the semiconductor conduction-band levels depends on how much population is being promoted to the molecular excited state from the ground state and how quickly this excited population is being transferred to the electrode. As the coupling $\hbar g$ is increased from zero, it helps to boost the population in the excited state, and one finds a corresponding growth in the enhancement of injected population. (In a classical picture, the local electric field enhancement near the molecule due to the presence of the plasmonic particle is approximately $g\mu_s/(\mu_m\gamma_s)$, i.e., proportional to g . This enhanced field then can boost the molecular transition probability through the molecular dipole-field coupling.) However, as $\hbar g$ increases further, de-excitation of the electronic population back to the ground state also increases. This is due to enhanced spontaneous emission, i.e., the Purcell effect, which can also be understood as energy transfer from electron excitations to plasmons excitations.¹⁸ (More explicitly, the coupling to the plasmon can be thought of as effectively adding a term $4g^2/\gamma_s$ to the spontaneous emission rate γ_e .¹⁵) For slower electron-transfer rates, as the value of $\hbar g$ is increased beyond the optimum value, a significant portion of the excited electronic population returns to the ground state before being transferred to the electrode, decreasing the injection efficiency. When the electron-transfer rate is high, it can continue to transfer the maximum possible EIP even as $\hbar g$ increases beyond the threshold value and thereby lead to the plateau behavior of EIP. High $\hbar g$ values lead to oscillations of electronic population between the ground and excited electronic states, damped by the plasmon relaxation/dephasing rate. A low plasmon relaxation/dephasing rate acts in a similar manner to an extremely rapid electron-transfer rate, in that it

allows for relatively undamped oscillation of population between excited and ground electronic states; this repeated repopulation of the excited state enables even a relatively slow electron-transfer rate to eventually transfer most of the electronic population to the electrode and thus ensures a long plateau of EIP for higher $\hbar g$ values (red triangles in Figure 2b). Realistic values of τ_{el} and γ_s likely correspond to a regime where there is an optimum value of coupling $\hbar g$ where EIP is maximized. In such cases, it is interesting to note that maximum injection efficiency is obtained only for a specific set of electron transfer and relaxation/dephasing rates, similar to the quantum Goldilocks effect suggested for exciton transport in photosynthetic antenna systems.¹⁹

The existence of an optimum or threshold coupling constant is due to modification of the coupled dynamics of the entire sensitizer-plasmon-semiconductor system. This means that the dynamics of electron injection will change as the coupling strength is changed, as shown in Figure 3a,b. (Note that the results in Figure 2b are extracted from the injection-dynamics data of Figure 3a,b, before the data are normalized.) In Figure 3a, for relatively fast plasmon relaxation, increasing the value of $\hbar g$ to 2.8 meV leads to a slight slowing of the injection time scale. Subsequent increases lead to faster and faster injection dynamics, indicating that the injection dynamics is no longer governed by τ_{el} and is strongly influenced by coupling to plasmons of the MNP. For the slower plasmon relaxation shown in Figure 3b, the injection dynamics are significantly different. As the value of the coupling $\hbar g$ is increased from zero, the injection dynamics immediately slow considerably. Further increases in coupling lead to faster electron injection, but even for very high values of $\hbar g \geq 50.8$ meV, it takes longer to complete the process of electron injection compared to the case of no plasmons. In both cases, as $\hbar g$ is increased, the electron-transfer time decreases. If the plasmon relaxation/dephasing rates are rapid, then electron injection times continue to get shorter and approach the duration of the laser pulse. If the plasmon relaxation/dephasing rates are low, the electron injection times saturate beyond a certain $\hbar g$ value. Increasing $\hbar g$ initially increases the population in the excited state, but that population takes longer to complete the transfer process. As $\hbar g$ is increased further, there is rapid promotion of electrons to the excited state and electrode states unless the plasmon relaxation/dephasing is very slow. Such a slow plasmon relaxation/dephasing rate means that the excited population is also rapidly transferred to the ground state, and transfer to

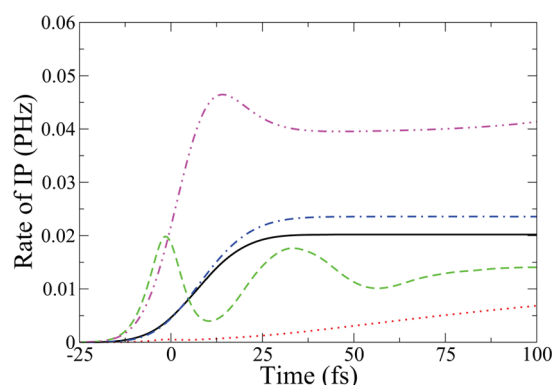


Figure 4. Rate of electron transfer as a function of time for $\tau_{el} = 50$ fs. $g = 0$ (solid black); $\hbar\gamma_s = 0.01$ meV, $\hbar g = 0.8$ meV (dotted red); $\hbar\gamma_s = 0.01$ meV, $\hbar g = 18.8$ meV (dashed green); $\hbar\gamma_s = 0.41$ meV, $\hbar g = 14.8$ meV (dot-dashed blue); $\hbar\gamma_s = 0.41$ meV, $\hbar g = 34.8$ meV (dot-dot-dashed magenta).

the electrode is resumed only after the excited state is repopulated as the electronic population oscillates between ground and excited state.

The rate of electron transfer is plotted as a function of time in Figure 4 to illustrate the effect of electron–plasmon coupling on electron-transfer dynamics in a more quantitative fashion. In order to compute the transfer rate, the time derivative of IP is computed and normalized by an appropriate factor. The case where $g = 0$ is shown as a dark solid line that correctly levels at long times at a value of 0.02 PHz (the inverse of $\tau_{el} = 50$ fs). The fact that at early times the electron injection rate τ_{el}^{-1} is different from this value, even for $g = 0$, is due to the effect of the state being populated by the laser pulse in a finite amount of time. Two curves relating to the slow plasmon dephasing case (Figure 3b) are shown to have much slower transfer rates that deviate significantly from a single exponential. Two curves from the fast plasmon dephasing case are seen to be more nearly single exponential, although the rates are much faster than for $g = 0$. These results thus indicate that, except for the case of slow plasmon dephasing, significant deviation from the $g = 0$ electron-transfer rates occurs only when the electron–plasmon coupling is well past the optimum or threshold value.

Electron–plasmon dynamics has been modeled and computed in this work without any explicit reference to temperature. Evidence from experimental data points to not just DSSC efficiencies being temperature independent,²⁰ but also the rate of the primary electron injection step remaining constant over a large temperature range.²¹ Earlier theoretical models¹⁷ have shown that by assuming (i) empty conduction band levels (i.e., the Fermi level is positioned within the band gap of the electrode); (ii) constant electronic coupling between the excited state and the electrode states; and (iii) uniform density of electrode states, electron-injection dynamics become temperature independent, even in the presence of inelastic injection due to the molecular vibrational modes. More detailed theoretical models of the electron injection process^{22–24} that use DFT methods to calculate electronic wave functions that are next propagated using a time-dependent Schrödinger wave equation approach, and that include vibrational modes, result in nonconstant electrode densities of states and nonconstant electronic coupling. However, results from these detailed theoretical models indicate that temperature effects are weak and can thus safely be neglected.²³ Plasmon dynamics can also reasonably be assumed to be temperature-independent. The

energy to excite a plasmon in this work is 2.02 eV, much higher than the operational temperature of any device, so the initial plasmon population can be taken to be entirely in its ground state. Plasmon dephasing rates depend linearly on temperature,²⁵ but this is unlikely to have a significant effect in the most likely scenario of a moderately strong coupling leading to fast electron transfer.

Direct tunneling of high-energy electrons from the MNP to the molecular levels or the electrode has not been considered in this work. Such pathways come into play when there is near or direct contact between MNP and electrode or molecular systems.²⁶ The mechanism of hot electron tunneling is usually preceded by plasmon break up into high-energy electron–hole pairs, but recent calculations also indicate that plasmons in MNP can delocalize directly into nearby electrodes, leading to direct electron injection.²⁷ We assume here that the MNP–electrode and MNP–sensitizer separations are large enough that these mechanisms do not come into play.²⁶

CONCLUSIONS

Starting from a fairly general Hamiltonian, and modeling the laser-induced dynamics using a density-matrix approach, we showed how coupling to MNP plasmons influences both the yield and the injection dynamics for electron transfer at photosensitized interfaces. The results indicate that the injection dynamics are influenced by coupling of electronic excitations with plasmons and that there exists either an optimum value of coupling for which the injection efficiency is maximum or a threshold coupling at which the injection efficiency is maximized and subsequently plateaus. This optimum or threshold value of the coupling emerges from an interplay between various competing processes, including electron transfer and the Purcell effect, and its precise value is thus influenced by electron transfer and plasmon relaxation/dephasing time scales. Future calculations will be devoted to verifying that an optimum value for the electronic–plasmon coupling persists when the system is excited using continuous-wave radiation with an intensity comparable to what would be experienced within a DSSC. We hope to also correlate the electronic–plasmon coupling, which was varied parametrically in this work, to the size and shape of the MNP, the dipole moment of the photosensitizer, and the relative arrangement of the photosensitizer and MNP, thereby establishing the conditions under which the optimum coupling can be achieved.

Experimental work so far has demonstrated that injection efficiencies can be increased or decreased by modifying the coupling value, but the existence of an optimum has been reported only in the context of plasmon-enhanced photocatalysis.²⁶ We hope that our theoretical results will motivate further experiments to find this optimum both in plasmon-mediated DSSC as well as in photocatalysis. Time-resolved laser spectroscopy, particularly transient-absorption measurements, could be used to verify the predicted modifications of electron injection dynamics.¹⁴ Finally, photoinduced electron transfer at interfaces is the fundamental physical process underlying not only DSSCs but also several other types of solar cells, including organic solar cells,²⁸ quantum dot solar cells,²⁹ and perovskite solar cells;³⁰ the ability to optimize the electron transfer and modify its dynamics may have important implications for these devices as well.

■ AUTHOR INFORMATION

Corresponding Author

*E-mail: t-seideman@northwestern.edu.

Notes

The authors declare no competing financial interest.

■ ACKNOWLEDGMENTS

T.S. thanks the National Science Foundation (Grant 1465201) for support of this research. This work was performed, in part, at the Center for Nanoscale Materials, a U.S. Department of Energy, Office of Science, Office of Basic Energy Sciences User Facility under Contract DE-AC02-06CH11357.

■ REFERENCES

- (1) Atwater, H. A.; Polman, A. Plasmonics for improved photovoltaic devices. *Nat. Mater.* **2010**, *9*, 205–13.
- (2) Notarianni, M.; Vernon, K.; Chou, A.; Aljada, M.; Liu, J.; Motta, N. Plasmonic effect of gold nanoparticles in organic solar cells. *Sol. Energy* **2014**, *106*, 23–37.
- (3) Choi, H.; Chen, W. T.; Kamat, P. V. Know thy nano neighbor. Plasmonic versus electron charging effects of metal nanoparticles in dye-sensitized solar cells. *ACS Nano* **2012**, *6*, 4418–4427.
- (4) Sheehan, S. W.; Noh, H.; Brudvig, G. W.; Cao, H.; Schmittenmaier, C. A. Plasmonic enhancement of dye-sensitized solar cells using core-shell-shell nanostructures. *J. Phys. Chem. C* **2013**, *117*, 927–934.
- (5) Jeong, N. C.; Prasittichai, C.; Hupp, J. T. Photocurrent enhancement by surface plasmon resonance of silver nanoparticles in highly porous dye-sensitized solar cells. *Langmuir* **2011**, *27*, 14609–14614.
- (6) Qi, J.; Dang, X.; Hammond, P. T.; Belcher, A. M. Highly efficient plasmon-enhanced dye-sensitized solar cells through metal@oxide core-shell nanostructure. *ACS Nano* **2011**, *5*, 7108–7116.
- (7) Brown, M. M. D.; Suteewong, T.; Kumar, R. S. S.; D'Innocenzo, V.; Petrozza, A.; Lee, M. M.; Wiesner, U.; Snaith, H. J. Plasmonic dye-sensitized solar cells using core-shell metal-insulator nanoparticles. *Nano Lett.* **2011**, *11*, 438–445.
- (8) Masiello, D. J. Multiscale theory and simulation of plasmon-enhanced molecular optical processes. *Int. J. Quantum Chem.* **2014**, *114*, 1413–1420.
- (9) Chen, H.; Blaber, M. G.; Standridge, S. D.; DeMarco, E. J.; Hupp, J. T.; Ratner, M. A.; Schatz, G. C. Computational modeling of plasmon-enhanced light absorption in a multicomponent dye sensitized solar cell. *J. Phys. Chem. C* **2012**, *116*, 10215–10221.
- (10) Wang, L.; May, V. Plasmon enhanced heterogeneous electron transfer: a model study. *J. Phys. Chem. C* **2014**, *118*, 2812–2819.
- (11) Wang, L.; May, V. Theory of plasmon enhanced interfacial electron transfer. *J. Phys.: Condens. Matter* **2015**, *27*, 134209.
- (12) Hagfeldt, A.; Boschloo, G.; Sun, L.; Kloo, L.; Pettersson, H. Dye-sensitized solar cells. *Chem. Rev.* **2010**, *110*, 6595–6663.
- (13) Labat, F.; Le Bahers, T.; Ciofini, I.; Adamo, C. First-principles modeling of dye-sensitized solar cells: Challenges and perspectives. *Acc. Chem. Res.* **2012**, *45*, 1268–1277.
- (14) Katoh, R.; Furube, A. Electron injection efficiency in dye-sensitized solar cells. *J. Photochem. Photobiol., C* **2014**, *20*, 1–16.
- (15) Shah, R. A.; Scherer, N. F.; Pelton, M.; Gray, S. K. Ultrafast reversal of a Fano resonance in a plasmon-exciton system. *Phys. Rev. B* **2013**, *88*, 075411.
- (16) Waks, E.; Sridharan, D. Cavity QED treatment of interactions between a metal nanoparticle and a dipole emitter. *Phys. Rev. A* **2010**, *82*, 043845.
- (17) Ramakrishna, S.; Willig, F.; May, V. Theory of ultrafast photoinduced heterogeneous electron transfer: Decay of vibrational coherence into a finite electronic-vibrational quasicontinuum. *J. Chem. Phys.* **2001**, *115*, 2743.
- (18) Pelton, M. Spontaneous emission modification in nanophotonic structures. *Nat. Photonics* **2015**, *9*, 427–435.
- (19) Rebertus, P.; Mohseni, M.; Kassal, I.; Lloyd, S.; Aspuru-Guzik, A. Environment-assisted quantum transport. *New J. Phys.* **2009**, *11*, 033003.
- (20) Grätzel, M. Dye-sensitized solar cells. *J. Photochem. Photobiol., C* **2003**, *4*, 145–153.
- (21) Watson, D. F.; Meyer, G. J. Electron injection at dye-sensitized semiconductor electrodes. *Annu. Rev. Phys. Chem.* **2005**, *56*, 119–156.
- (22) Abuabara, S. G.; Rego, L. G. C.; Batista, V. S. Influence of thermal fluctuations on interfacial electron transfer in functionalized TiO₂ semiconductors. *J. Am. Chem. Soc.* **2005**, *127*, 18234–18242.
- (23) Duncan, W. R.; Prezhdo, O. V. Temperature independence of the photoinduced electron injection in dye-sensitized TiO₂ rationalized by ab initio time-domain density functional theory. *J. Am. Chem. Soc.* **2008**, *130*, 9756–9762.
- (24) Li, J.; Kondov, I.; Wang, H.; Thoss, M. Quantum dynamical simulation of photoinduced electron transfer processes in dye-semiconductor systems: theory and application to coumarin 343 at TiO₂. *J. Phys.: Condens. Matter* **2015**, *27*, 134202.
- (25) Liu, M.; Pelton, M.; Guyot-Sionnest, P. Reduced damping of surface plasmons at low temperatures. *Phys. Rev. B* **2009**, *79*, 035418.
- (26) Linic, S.; Christopher, P.; Ingram, D. B. Plasmonic-metal nanostructures for efficient conversion of solar to chemical energy. *Nat. Mater.* **2011**, *10*, 911–921.
- (27) Long, R.; Prezhdo, O. V. Instantaneous generation of charge-separated state on TiO₂ surface sensitized with plasmonic nanoparticles. *J. Am. Chem. Soc.* **2014**, *136*, 4343–4354.
- (28) Günes, S.; Neugebauer, H.; Sariciftci, N. S. Conjugated polymer-based organic solar cells. *Chem. Rev.* **2007**, *107*, 1324–1338.
- (29) Kamat, P. V. Quantum dot solar cells. Semiconductor nanocrystals as light harvesters. *J. Phys. Chem. C* **2008**, *112*, 18737–18753.
- (30) Green, M. A.; Ho-Baillie, A.; Snaith, H. J. The emergence of perovskite solar cells. *Nat. Photonics* **2014**, *8*, 506–514.